Title: A Boron-Coated Ionization Chamber for Ultra-Cold 1 Neutron Detection

Author(s):
Salvat, Daniel J.
Adamek, Evan R.
Bacon, Jeffrey D.
Hoagland, Jeffrey C.
Holley, Adam T
Liu, Chen-Yu
Makela, Mark F.
Morris, Christopher
Ramsey, John C.
Reid, Austin R.
Rios, Raymond
Saunders, Alexander
Sjue, Sky K.
Vorndick, Brittney M.
Wang, Zhehui
Young, Albert R.

Intended for: Nuclear Instruments and Methods in Physics Research A
A

A Boron-Coated Ionization Chamber for Ultra-Cold Neutron Detection

D.J. Salvat[a,*], E.R. Adamek[a], C.-Y. Liu[a], J. Bacon[b], M. Makela[b], C.L. Morris[b], J. Ramsey[b], A. Saunders[b], S.K.L. Sjue[b], Z. Wang[b], R. Rios[c], J. Hoagland[d], A.T. Holley[d], A. Reid[d], B. VornDick[d], A.R. Young[d]

[a] *Indiana University Center for Exploration of Energy and Matter, Bloomington, IN 47408, USA*
[b] *Los Alamos National Laboratory, Los Alamos, NM 87544, USA*
[c] *Idaho State University, Pocatello, ID 83209, USA*
[d] *North Carolina State University, Raleigh, NC 27695, USA*

Abstract

The design and characterization of a boron-coated ionization chamber for the detection of ultra-cold neutrons (UCN) are presented. A spray-coated ^{10}B powder layer provides an inexpensive and simple alternative to ^{3}He gas as a neutron absorber. Results using UCN from the solid deuterium UCN source at the Los Alamos Neutron Science Center indicate comparable efficiency to ^{3}He ionization chambers and proportional counters currently used at the UCN source. In addition, the ion chamber is used to detect thermal neutrons. A comparison of the thermal neutron and UCN pulse-height spectra suggests that UCN only capture near the layer surface.

Keywords: ionization chamber, ultracold neutrons, helium-3 replacement, boron-10, powder coating

*corresponding author
Email address: dsalvat@indiana.edu (D.J. Salvat)

1. Introduction

Slow neutrons interact with matter primarily by scattering from the nuclei of the material. Because slow neutron wavelengths are much larger than the size of a nucleus, the nucleus can be described by a hard-core potential[1]. For wavelengths larger than the intermolecular spacing in a material, it suffices to spatially average the hard-core potential over all nuclear sites. This leads to a uniform, effective potential for materials, which is proportional to the material's coherent scattering length[2]:

$$V_f = 2\pi\hbar^2 m^{-1} nb. \tag{1}$$

Here, m is the neutron mass, n is the number density of the material, and b is the material's coherent scattering length. Neutrons with an energy less than V_f can be reflected from the material. If b is complex due to nuclear absorption of neutrons, the potential contains both real and imaginary terms so that $V_f = V - iW$. We can define $f \equiv W/V$ which is related to the probability of absorption for each reflection from the material surface. For many materials, V_f is on the order of 100 neV, and f is on the order of 10^{-5}. One can thus trap neutrons in this energy regime within material volumes with relatively low losses. These neutrons are referred to as Ultra-Cold Neutrons (UCN), and they have led to an extensive arena for the study of the neutron's properties: for example, the most precise measurements of the neutron beta decay lifetime and electric dipole moment are performed using UCN[3, 4].

Proportional chambers filled with ^{3}He gas provide a simple means to count UCN[5]. Neutrons capture on helium via ^{3}He(n,p)t, with a Q value of 0.764 MeV. The resulting proton and triton ionize a stopping gas which has a small neutron absorption cross section for neutrons, such as CF_4 or Ar. The current shortage of ^{3}He may limit the use of these detectors for future UCN experiments[6].

^{10}B provides an alternative to ^{3}He. Ions are produced through the neutron-capture reaction ^{10}B(n,α)^{7}Li, with a Q value of 2.8 MeV. 94% of the reactions leave the ^{7}Li in an excited state, which decays to the ground state with the release of a 0.48 MeV photon. The neutron capture cross section for ^{10}B is about 72% of that for ^{3}He[7].

Boron can be used as an absorber in the form of a solid ^{10}B powder layer on the inner surface of a gaseous detector. Neutrons capture on the solid layer, and either the Li or α ionizes gas in the detector volume. Recently, commercially available boron-lined GEM detectors have been used for UCN experiments[8]. The use of solid boron suffers from a potential disadvantage compared to gaseous neutron absorbers: the daughter Li and α ions have short ($\sim 2\mu$m) ranges in the boron layer, causing additional energy loss prior to entering the gas volume, and thus reducing the detection efficiency. To our knowledge, the severity of this effect for UCN remains undiscussed in the literature.

In this work, we apply a boron coating previously used in thermal neutron detectors[9]. The boron is spray-coated on the interior walls of a cylindrical ionization chamber; UCN enter through an aluminum window, capture on the boron layer, and ionize CF_4 gas within the detector volume. Our data suggests that UCN interact with only the outer surface of the coating, mitigating the ion energy loss in the solid. This permits a UCN detection efficiency comparable to a ^{3}He ion chamber.

2. Design

The chassis of the ion chamber consists of a 7.620 cm long stainless steel tube, with a 7.620 cm outer-diameter and 1.65 mm thick walls (see figure 1). A vacuum port and high-voltage feedthrough are connected to one side, and a 0.51 mm thick aluminum window is fastened between the tube and a polyoxymethylene cap, which electrically isolates the detector from UCN guides and vacuum components. The anode is a single 4.76 mm thick copper conductor, protruding 5.080 cm into the cylindrical volume. The detector is pumped and filled with gas through a welded VCR feedthrough.

To make the boron coating, 0.0575($\pm$30%) g of ^{10}B powder (>97% isotopic purity) is mixed into an acetone and polystyrene (4 mg) solution, and the mixture is sprayed manually in three coats throughout the interior of the detector volume. The smoothness and uniformity of the coating are not characterized. We estimate the layer thickness to be 1.54 ± 0.46 μm, assuming that the coating is distributed evenly on the detector walls. The ^{10}B capture cross section is 3835 barns at 2200 m/s. At a number density of 1.31×10^{23}cm^{-3}, the mean-free path $\ell \equiv (n\sigma)^{-1}$ is 27 nm for 3 m/s UCN. As such, UCN cannot penetrate deep into the boron layer.

Pure ^{10}B has $b = -0.1 - 1.066i$, so that $V_f = -3.41 - 36.4i$ neV. With 3% of ^{11}B ($b = 6.65$), the net potential is $3.50 - 36.4i$ neV. For this Fermi potential, the probability of reflection per bounce averaged over all angles of reflection θ gives 15% for 50 neV UCN. The effect of surface roughness will

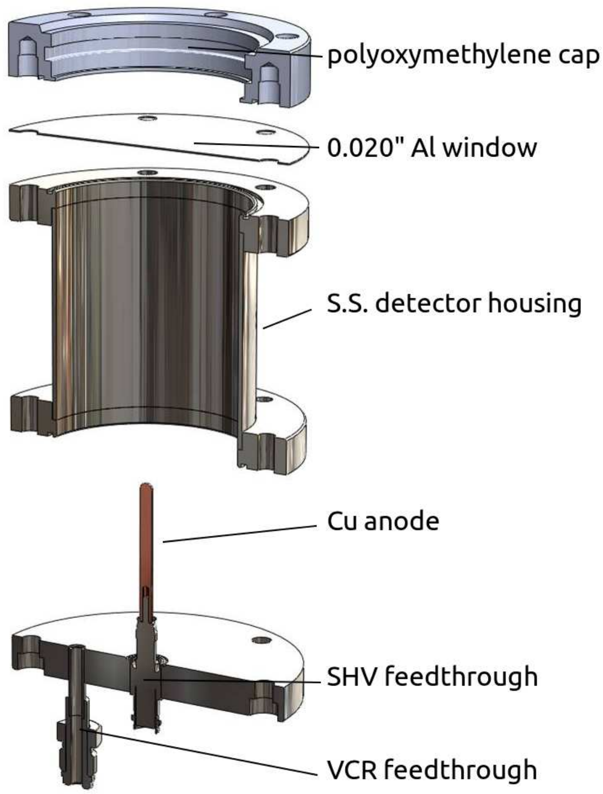

Figure 1: A schematic of the UCN detector assembly. The bottom plate, aluminum window, and polyoxymethylene cap are sealed with o-rings.

only decrease this value [2].

3. Methods

We compare the performance of the boron-coated detector to the same detector housing filled with 10 mbar of ^{3}He. Both detectors are filled with 500 mbar of CF_4 gas. The anode is biased to 500 Volts, and pulses are collected using charge-sensitive preamplifiers. The pulses are then amplified by spectroscopy amplifiers with a 6 μs time constant and read into a multichannel analyzer.

At a density of 0.0393 g/cc for CF_4 at 500 mbar and and 300 Kelvin, the ranges of the charged particles (estimated using SRIM2008 code[10]) are 6.13 mm for 1.47 MeV alpha, 7.35 mm for 1.78 MeV alpha, 3.44 mm for 0.85 MeV ^{7}Li, and 3.83 mm for 1.02 MeV ^{7}Li. The ranges are much smaller than the gap between the anode and the wall, allowing full deposition of the charged particle energies in the gas.

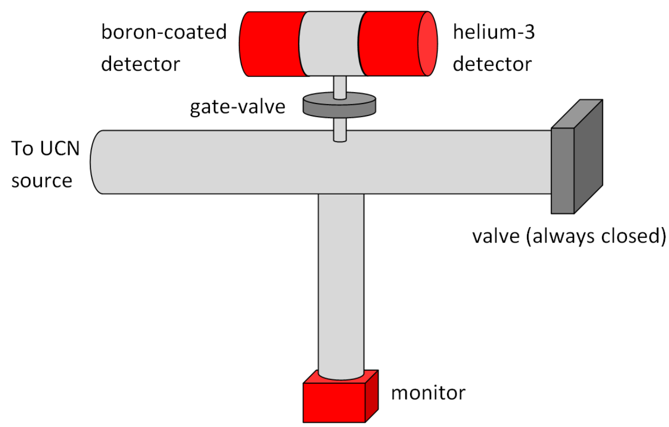

Figure 2: The detector mount configuration. Lengths are not to scale.

To acquire data using UCN, the helium and boron-coated detectors are fastened to either side of an electro-polished guide tee and mounted on top of a gate valve, below which is a UCN guide leading to the solid deuterium source. The gate valve is closed to measure the background rate of the detectors. A small aperture on the underside of the UCN guide leads downward to a multi-wire proportional counter used to monitor the incoming flux of UCN. This configuration is shown in figure 2. Data are also acquired using a ^{252}Cf neutron source moderated with room temperature polyethylene.

4. Results

Figure 3 shows a comparison of the pulse height spectra for the helium and boron-coated detectors. Because neutrons capture on the wall of the boron detector, either the Li or α will ionize the gas, and there is no full-energy peak. We are thus left with two prominent edges corresponding to the full energy of each ion. There is a less intense higher energy edge due to α ions from the 6% decay branch.

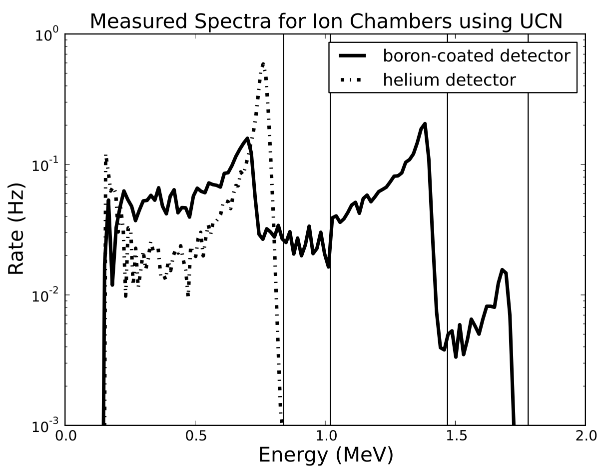

Figure 3: Pulse-height spectra for the helium and boron-coated ionization chambers using UCN. The vertical lines represent the Li and α energies of 0.84, 1.02, 1.47, and 1.78 MeV.

To measure the relative detector efficiencies of the helium and boron-coated designs, data are acquired simultaneously for both detectors. The spectrum for each detector is measured with the gate valve open, and measured with the gate valve closed to determine the background spectrum. The signal spectrum is formed by normalizing all counts to the monitor rate, and subtracting the closed-valve spectrum from the open-valve spectrum. The energy calibration is performed by introducing an additional 5 mbar of ^{3}He into the boron detector, and using the known ^{3}He peak value of 0.764 MeV. In addition, counts below 0.15 MeV are discriminated, as γ-ray backgrounds from neutron capture are potentially high in this energy range. The ratio of the helium detector signal to the boron-coated detector signal is $(94 \pm 8)\,\%$. The error includes the propagated statistical uncertainty in the background spectra, as well as an estimated uncertainty in establishing the discrimination threshhold.

The discriminated count rate versus voltage for the boron-coated detector is shown in figure 4. The saturated ion region is reached for applied biases above 300 V.

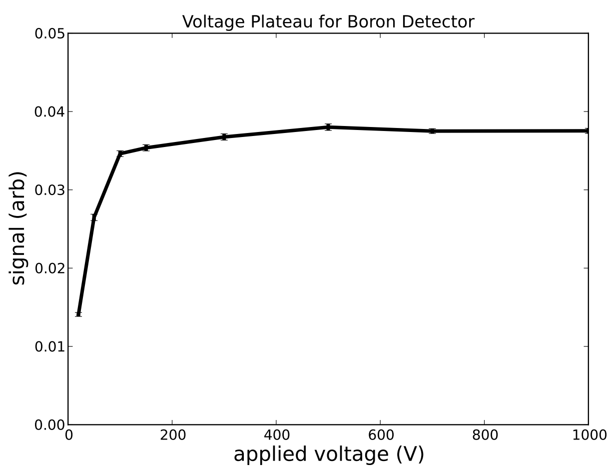

Figure 4: The discriminated pulse height spectrum for various applied biases. The discrimination threshhold is adjusted for each voltage.

Finally, figure 5 compares the pulse-height spectra of the boron counter using UCN and thermal neutrons. The full energy peaks are wider using thermal neutrons: faster neutrons can penetrate further into the boron layer than UCN, and the subsequent ions must traverse a significantly larger portion of the coating, removing more energy prior to ionization in the gas. This will be discussed quantitatively in the next section.

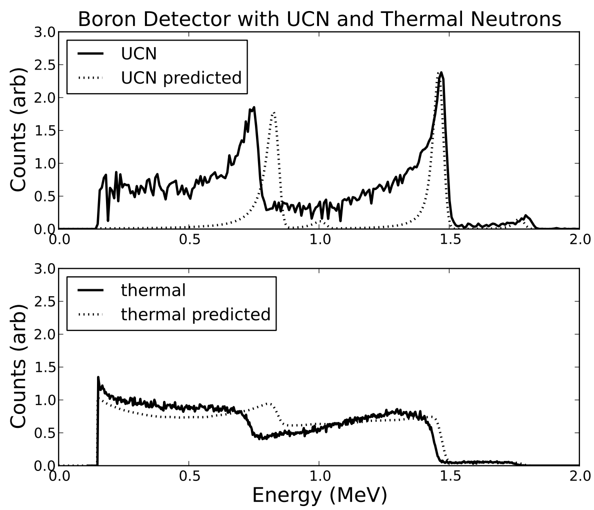

Figure 5: Comparison of boron-coated detector spectra for UCN and thermal neutrons. The spectra are scaled so that their integral is unity. The predictions are discussed in the next section.

5. Discussion

The efficiency of either detector can be written schematically as

$$\epsilon = \epsilon_{window}\epsilon_{abs}\epsilon_{gas}\epsilon_{ion}. \tag{2}$$

ϵ_{window} is the efficiency with which UCN can penetrate the front aluminum window, ϵ_{gas} the efficiency with which neutrons traverse the CF_4 volume without being up-scattered or absorbed, ϵ_{abs} the efficiency of neutron capture in the ^{10}B or ^{3}He, and ϵ_{ion} the efficiency of ion collection. We estimate the relative efficiency assuming that only ϵ_{abs} will differ between the detectors.

The probability of neutron capture in the ^{3}He gas is given by

$$\epsilon_{abs} = 1 - \exp\left(-x/\ell\right) \tag{3}$$

where $\ell = 1/\sigma_a n$ is the absorption mean-free path, and x is the path length of the neutron within the detector prior to capture on the boron-layer. We take the number density to be that of 10 mbar of ^{3}He gas at 300 Kelvin. Given the above, the mean-free path of a 100 neV UCN is 1.6 cm, or considerably less than the 7.6 cm detector length, giving a capture probability of 99%.

We proceed as is done previously to compute the absorption efficiency of the ^{10}B-coated detector[9]. We only consider the back-scatter case, where a neutron is incident upon the layer from with the detector volume, captures on a ^{10}B nucleus, and the resulting ion re-enters the volume. Assuming that the layer thickness is less than the ion ranges, the detection efficiency for either ion is given by[9]:

$$\begin{aligned} \epsilon_{boron} &= \frac{1}{2}\left(1 - \exp\left(-\frac{T}{\ell}\right)\right)\left(1 - \frac{\ell}{R_0}\right) \\ &\quad + \frac{T}{2R_0}\exp\left(-\frac{T}{\ell}\right). \end{aligned} \tag{4}$$

Here, T is the layer thickness, and R_0 is the range of either the α or Li ion in ^{10}B. The respective ranges of the α and Li are 3.6 and 1.9 μm for the 94% decay branch, and 4.4 and 2.2 μm for the 6% branch. We sum the efficiencies of both ions over both decay branches. In all cases, ℓ is much smaller than

R_0 and T, giving an efficiency for 100 neV neutrons of 98%. We therefore expect the total efficiencies of both detectors to be comparable.

We can understand the pulse-height spectra for the thermal neutron and UCN spectra as follows. The measured spectrum for a single ion is given by the number of ions, with an initial depth x and angle to the normal of the surface θ, that escape the layer such that their final energy is E. This is

$$\begin{aligned} \frac{dN}{dE} &= N_0 \int_0^1 d(\cos\theta) \int_0^\infty dx \\ &\times P(x,\cos\theta)\delta\left(E - \eta\left(x/\cos\theta\right)\right). \end{aligned} \tag{5}$$

Here, η is the final ion energy given an initial depth x and angle θ, and is given by

$$\eta = E_0 - \int_0^{x/\cos\theta} \frac{dE}{dL} \cdot dL \tag{6}$$

with E_0 being the initial ion energy. Further, P is the probability of an ion starting at a depth x and and angle θ within the layer, and is given by

$$P dx d(\cos\theta) = \lambda^{-1} \exp\left(-x/\lambda\right) dx d(\cos\theta) \tag{7}$$

where $\lambda = 1/\sigma_a n$ is the mean free path of the neutron incident on the boron layer. Note that the expression vanishes unless $E < E_0$, as otherwise the argument of the delta function has no roots in the domain of integration.

For ion energies slightly less than the full energy peak, η is small, and the ion range is much larger than the distance traversed in the layer. Thus, for ions at these energies, the energy loss in the layer is approximately constant:

$$-\frac{dE}{dL} \approx C \tag{8}$$

where $C > 0$. With this, integration over x and $\cos\theta$ gives

$$\frac{dN}{dE} = \frac{\lambda C + \exp\left(\frac{E-E_0}{\lambda C}\right)(E - E_0 - \lambda C)}{(E - E_0)^2}. \tag{9}$$

To illustrate the difference between the thermal and UCN data, we can compute the broadening of the full energy peak due to the energy loss in the boron. The width of dN/dE about E_0 is

$$W^2 = \int_0^{E_0} (E - E_0)^2 \frac{dN}{dE} \cdot dE \tag{10}$$

which leads to the expression

$$\begin{aligned} W^2 &= \lambda C \left[(E_0 + 2\lambda C) \exp(-E_0/\lambda C) \right. \\ &\quad \left. + E_0 - 2\lambda C\right]. \end{aligned} \tag{11}$$

From this, we see that the width approaches zero with decreasing λ, so that 3 m/s UCN, which have $\lambda \sim 27$ nm, will produce narrower peaks than 2200 m/s thermal neutrons ($\lambda \sim 20\mu$m).

The above describes the qualitative behavior of the measured spectra. However, measured counts at energies much lower than a full energy peak do not exhibit constant energy loss, and a more realistic model for dE/dL in the boron layer must be used for a more accurate description. In addition, the ^{3}He detector spectrum indicates a full energy peak resolution of 2%. This width is most probably due to shot noise and intrinsic instrumental resolution, and must be included in a prediction of the pulse-height spectrum for the boron detector.

To this end, we use the predicted values of dE/dL for Li and α ions in CF_4 gass at 500 mbar from SRIM2008 (see figure 6). The curves are

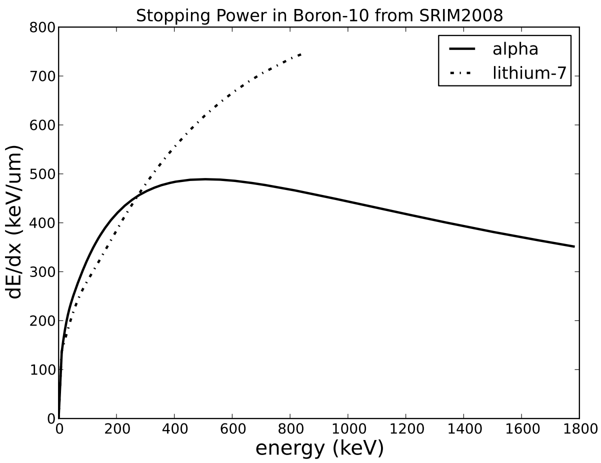

Figure 6: The stopping power of the ^{10}B layer for Li and α ions from SRIM2008.

integrated to find η for the Li and α ions, with E_0 the initial ion energies. Figure 7 shows the remaining ion energy versus distance traveled in the boron layer. With these quantities, equation (5) is integrated numerically to find the pulse-height distribution for each ion, and each decay branch. The calculation is performed with a layer thickness of 1.54μm, for both $\lambda = 27$ nm and $\lambda = 20\mu$m. The peaks are then convolved with a gaussian of width 0.015 keV, commensurate with the width of the full energy peak for the ^{3}He pulse height spectrum. Finally, the individual peaks are weighted by their respective branching ratios, and combined to form the complete spectrum. The results of this calculation are shown in figure 5.

The model presented captures the salient features of the measured spectra. There are, however, an excess of counts below the full energy peaks in the UCN data which are not predicted by the model. The cause of this is unknown at this time, though it is unimportant insofar as it does not effect

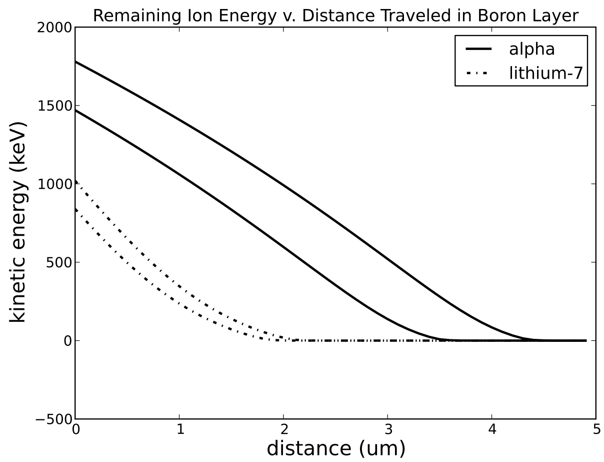

Figure 7: The energy of the ions in the boron-10 layer as a function of their distance traveled. The two curves for each ion correspond to the two initial ion energies for the 94% and 6% decay branches.

the total efficiency of the detector compared to the ^{3}He ion chamber. The surface roughness of the layer may locally screen the applied electric field, causing extra recombination, and thus counts well below the full energy peak.

It is further evident from figure 5 that the the full energy Li peaks are measured to be 10% lower than their expected values. The ion energy loss per ion pair created (W-value) of α ions in CF_4 is known to be a somewhat high 34.3 eV/ion compared to the first ionization potential of $\sim$ 15eV[11]. This is due to electron impact induced dissociation of CF_4 molecules in the gas. Any dependence of the W-value on the incident ion may cause differing amounts of extra energy loss in the gas, and thus a shift in the relative full energy peak positions for the Li ions.

6. Conclusions

The spray-coated boron ion chamber provides an effective and inexpensive means to count UCN. The implementation of these detectors at the LANSCE UCN source will greatly reduce our dependence on ^{3}He, and our results indicate a comparable efficiency to previously used ^{3}He ion chambers.

Our comparison of UCN and thermal neutron data suggests that UCN only interact with the surface of the boron coating. However, further characterization of the rougness and thickness of the boron coating is necessary to provide a more detailed understanding of the pulse-height spectrum.

7. Acknowledgements

The UCN facility at LANSCE is supported by DOE and LANL LDRD programs. In addition, DJS is supported in part by the DOE Office of Science Graduate Fellowship Program administered by the Oak Ridge Institute for Science and Education (ORISE).

[1] M.L. Goldberger, F. Seitz, Phys. Rev. 71 (1947) 294–310.

[2] R. Golub, D. Richardson, S.K. Lamoreaux, Ultracold Neutrons, first ed., Taylor & Francis, 1991.

[3] C.A. Baker, et al, Phys. Rev. 97 (131801).

[4] S. Arzumanov, et al, Phys. Rev. Lett. B 483 (1-3) (2000) 15–22.

[5] C.L. Morris, et al, Nucl. Inst. and Meth. A 599 (2009) 248–250.

[6] R.L. Kouzes, Pacific Northwest National Laboratory Report PNNL-18388 (2009).

[7] G.F. Knoll, Radiation Detection and Measurement, fourh ed., Wiley, 2010.

[8] P. Geltenbort, et al, Nucl. Inst. and Meth. A 642 (2010) 168–172.

[9] Z. Wang, C.L. Morris, Nucl. Inst. and Meth. A 652 (2011) 323–325.

[10] Http://www.srim.org. Accessed 9 December 2011.

[11] G.F. Reinking, et al, J. Appl. Phys. 60, 499 (1986).